A Search for Homogeneous Samples of Quasars

Volker Gericke
Astronomisches Institut
Westfälische Wilhelms-Universität
Münster, F.R. Germany

Abstract

An automated search for quasars, based on MRSP software, is applied to low-dispersion objective prism plates. Two criteria are used. The first criterion is the UV excess of low and medium redshift quasars. The second criterion is the presence of emission lines. 25 000 non-overlapping spectra in the ESO/SRC field No. 411 were analyzed; 600 show UV excess, 2 500 spectra have apparent emission lines. Both criteria taken separately lead to a large number of "false" objects. In the combined feature space known quasars occupy a characteristic region. Among the objects from this region in the limited magnitude range $18^m - 19^m$ 600 quasar candidates were found. Redshifts were determined from the low-dispersion objective prism spectra for 255 of these objects. The spatial distribution of 158 Ly α quasars is discussed.

1 Introduction

When normal galaxies are used to study large scale structures in the universe, only data up to redshifts $z = 1$ are available so far. With quasars it is possible to investigate large scale distributions of luminous matter at distances up to $z = 4$ and beyond.

To date, two quasar catalogues exist; both list the majority of the approximately 3 500 known quasars distributed over the whole sphere (Hewitt and Burbidge 1987, Véron-Cetty and Véron 1987). The catalogues contain very inhomogeneous data, because they include the results of different authors using different techniques to find and to identify quasars. Some spectra are obtained through slit spectroscopy, others from objective prism plates, leading to different degrees of reliability of the redshifts listed. In some cases the origin of the quoted redshifts remains unclear.

Several *automated* quasar surveys, intended to increase the number of known objects, are in progress. The first automated procedures were employed by Clowes *et al.* (1984) and Hewett *et al.* (1985). More recent work based on very low dispersion objective prism spectra is reported by Beuermann and Clowes (1988). A survey using somewhat higher dispersion spectra was started in Hamburg and is presented by Hagen *et al.* (1988). Automated procedures applied to low-dispersion objective prism spectra in Cambridge have led to remarkable results (Foltz *et al.* 1987). The present contribution concerns the automated search for quasars as part of the MRSP.

The ESO/SRC field No. 411 was investigated, with MRSP software applied to a film copy of the direct atlas J-plate and to the film copy of a low dispersion objective prism plate ($240\,\mathrm{nm\,mm^{-1}}$) taken in this region. The preprocessing of direct plates and

corresponding objective prism plates is described by Horstmann (1988) and Schuecker (1988). The criteria used for the automated quasar search are discussed in Sects. 2 to 4.

2 The UV-excess criterion

For the UV-excess excess criterion of low and medium redshift quasars, the center of intensity X_C of each spectrum is calculated:

$$X_C = \frac{\sum_{i=1}^{n} I_i X_i}{\sum_{i=1}^{n} I_i} \,. \tag{1}$$

The summations are taken over all pixels n of each spectrum. I_i is the intensity at pixel i; x_i is its position.

X_C values and magnitudes determine the feature space shown in *Fig. 1*. Small values of X_C correspond to red objects, high values to blue ones. Faint objects are located in the lower part of the diagram. Most objects lie on a 'main sequence'. Quasars which are found in the abovementioned catalogues are marked by squares.

Many of the quasars are found outside the 'main sequence', but the QSOs extend into the region of (normal) stars. This is due to the fact that the excess criterion

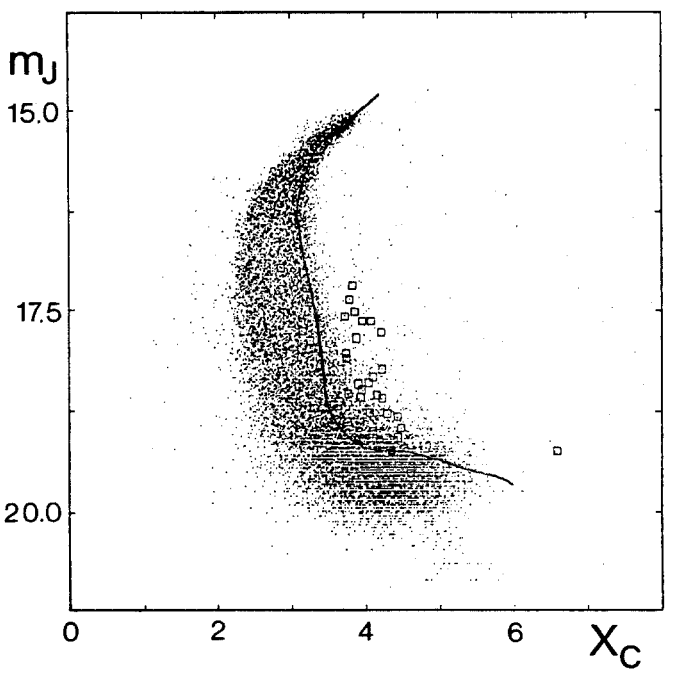

Fig. 1. PDS m_J magnitudes *vs.* center of intensity X_C. Large values of X_C correspond to blue objects. Quasars listed in the catalogues of Hewitt and Burbidge (1987) and Véron-Cetty and Véron (1987) are shown as squares.

is continuous, so that blue stars and relatively red quasars overlap. In low-density spectra the mixing results from blurring due to noise. A small percentage of the effect may also be due to possible misidentifications in the catalogues, with stars in the range G – M listed as quasars.

A random sample was taken from the region on the blue side of the linear discriminant, indicated in the diagram. The discriminant was determined by setting knots interactively and fitting a cubic spline function. The sample includes few quasars. From a total of 596 blue starlike objects only 82 are high probability quasar candidates as indicated by their clearly non-stellar continua and emission lines.

No quasars were found on the red side of the feature space.

3 The emission line criterion

To locate possible emission lines, the spectra between 350 nm and 520 nm are transformed to a linear wavelength scale. The fact that through this process the noise becomes nonrandom (wavelength dependent) is tolerated, though it restricts the recognition of emission lines to *strong* lines. The spectral intensities are corrected for atmospheric and instrumental extinction and for the sensitivity of the emulsion using the curves from Clowes *et al.* (1980). By these procedures the widths of the lines are directly comparable.

For each spectrum the positions $P_i^{\max}$ and the intensities $I(P_i^{\max})$ of all maxima are calculated, *i.e.* in the beginning of the calculations each peak is considered a possible emission line. The maxima are found from second derivatives calculated using Lagrangian polynomials. Best results are obtained for polynomials with 5 knots separated by $H = 6.8$ nm. The second derivative of the central knot is calculated by

$$I_3'' = \frac{1}{24H^2}\left(-2I_1 + 32I_2 - 60I_3 + 32I_4 - 2I_5\right) . \tag{2}$$

I_k is the intensity of the k^{th} knot. The constants are weighting factors, determined from the theory of Lagrangian polynomials. Calculating the second derivative acts as a filter of width H, because the value for the central knot is determined by the values of the side knots. The values of the second derivatives at the edges of the spectra are calculated with similar formulae, but lower accuracy. In this way the second derivative is obtained for each pixel.

During the next step the height and the width of each emission feature is determined. To calculate the height the continuum must be known. The points of inflection P_i^1 and P_i^2 below each maximum are determined; I_i^m, the mean value of the intensities at the two points, is used to determine the continuum I_i^C in the vicinity of each emission feature:

$$I_i^C = I_i^m - \left(I(P_i^{\max}) - I_i^m\right) . \tag{3}$$

The relative height I_i^r of an emission feature is

$$I_i^r = \frac{I(P_i^{\max}) - I_i^C}{I_i^C} . \tag{4}$$

The distance W_i between P_i^1 and P_i^2 is a measure of width:

$$W_i = |P_i^1 - P_i^2| \,. \tag{5}$$

In the corresponding feature space (*Fig. 2*), the intensity of the highest emission peak I_M of each spectrum is plotted *vs.* the width W_M of the same emission feature. Known quasars from the catalogues are again marked by squares. Peaks occur at multiples of the filter width H. The first peak at $W_M = 6.8\,\text{nm}$ contains all emission-like structures with W_M of the order of H. This peak is largely due to noise, though it includes also the narrow line quasars. The second peak at $W_M = 13.6\,\text{nm}$ includes all emission features with W_M of the order of $2H$. They are often due to real emissions, continuum features and emission lines. A third, very weak peak can be seen around $W_M = 20.4\,nm$. These features are caused by changes in the continuum.

The existence of more than one peak shows that the height of a spectral feature alone is not a sufficient characteristic for an emission line.

A sample taken from the region around $W_M = 13.6\,\text{mn}$ which is marked by the rectangle, leads to about 2 500 objects with apparent emission lines. Only a few of them are quasars. Objects with strong absorption breaks are found here because they feign emission lines. The most prominent absorption objects in this sample are G- and K-type stars, with a strong continuum hump between the G-band and the Ca II-break. Very red stars with narrow red contina simulate single-emission line objects.

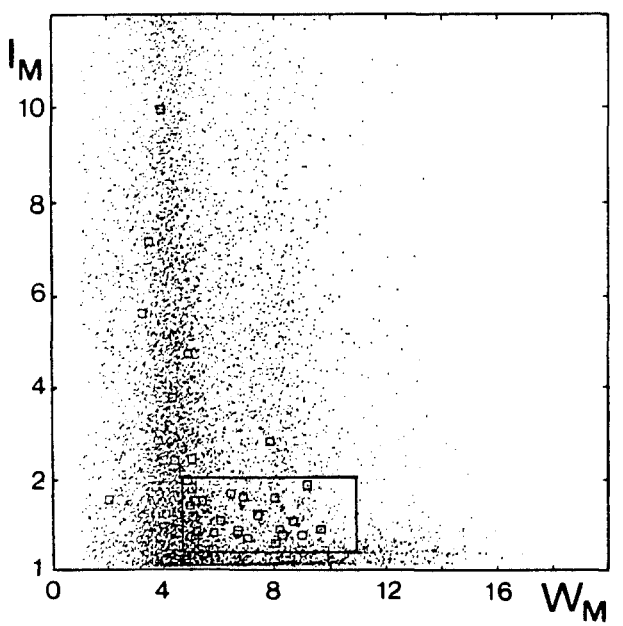

Fig. 2. Height I_M of the maximum emission feature *vs.* its width W_M. Quasars listed in the catalogues are shown as squares.

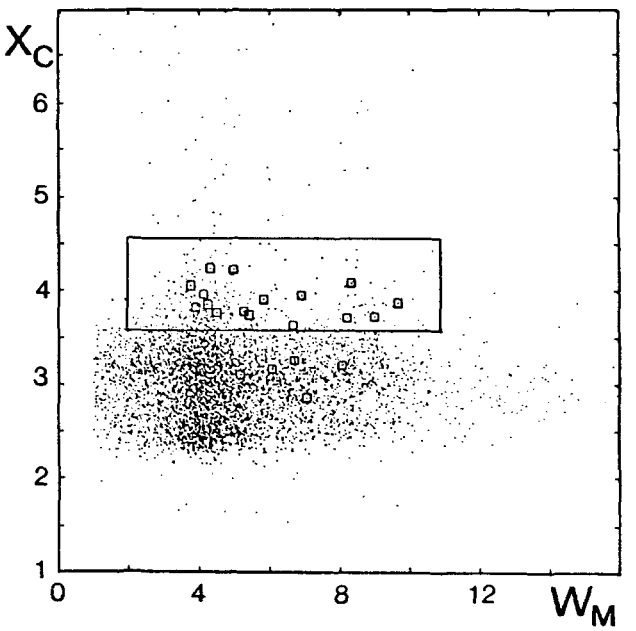

Fig. 3. Center of intensity X_C *vs.* width W_M of the highest peak in the magnitude range $18^m - 19^m$. Quasars listed in the catalogues are shown as squares.

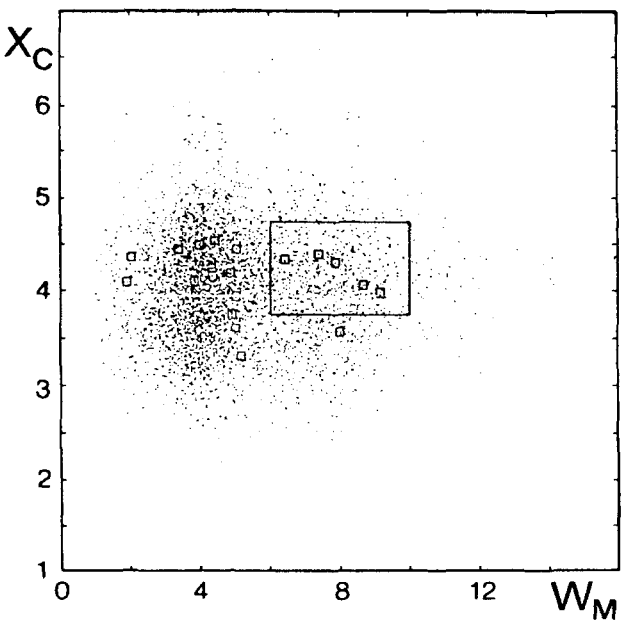

Fig. 4. Center of intensity X_C *vs.* width W_M of the highest peak in the magnitude range $19^m - 20^m$. Quasars listed in the catalogues are shown as squares.

4 The combined feature space

The UV-excess criterion and the emission line criterion taken separately do not suffice to unambiguously identify quasars. A more efficient way to locate quasars is the combination of two or more criteria. The two criteria discussed above can be combined in a new feature space with center of intensity X_C *vs.* width W_M of the highest emission feature. In *Fig. 3* the combined feature space includes all objects in the magnitude range $18^m - 19^m$. The separation between quasars and other starlike objects is clearly more apparent than in the cases where only one criterion was used. A sample of 600 objects is taken from the region extending above $X_C = 392\,\text{nm}$ (marked by a rectangle). Among these are only 5 % which can be *excluded* as quasars from a visual inspection of their objective prism spectra.

Figure 4 shows the combined feature space in the magnitude range between $19^m - 20^m$. The separation between quasars and other starlike objects is not as good as in the case of *Fig. 3* because of the higher noise in the spectra. About 600 objects are selected from the region around $W_M = 13.6\,\text{nm}$, marked by the rectangle. Only a few of the quasar candidates can be excluded to be quasars. But for faint objects it is much more difficult to confirm objects as quasars, because of the weak continua and the numerous spurious emission features.

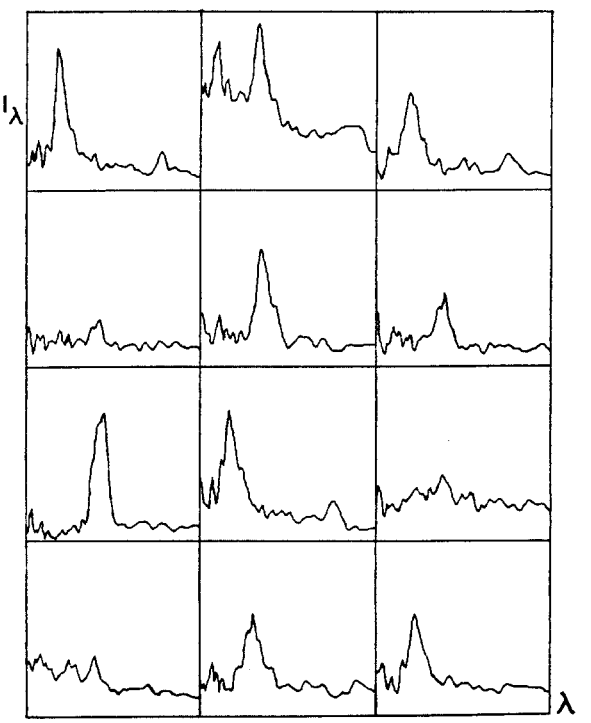

Fig. 5. Objective prism spectra of Ly α quasars found in this survey, intensity-corrected and on a linear wavelength scale.

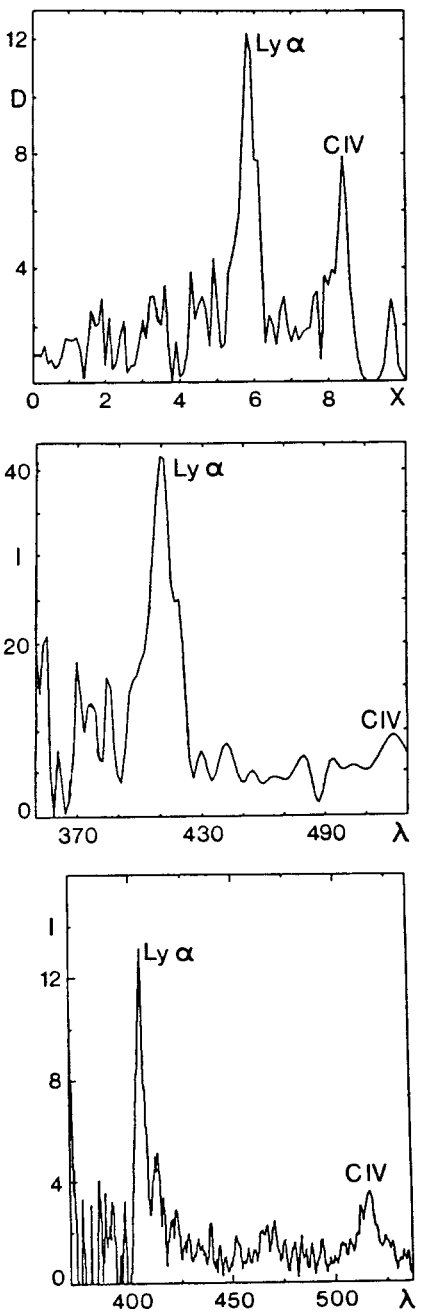

Fig. 6. Spectra of the quasar 0054-29, from top to bottom:
a) density spectrum (objective prism plate)
b) intensity corrected spectrum on a linear wavelength scale (objective prism plate)
c) slit spectrum (EFOSC, ESO 3.6 m-telescope).

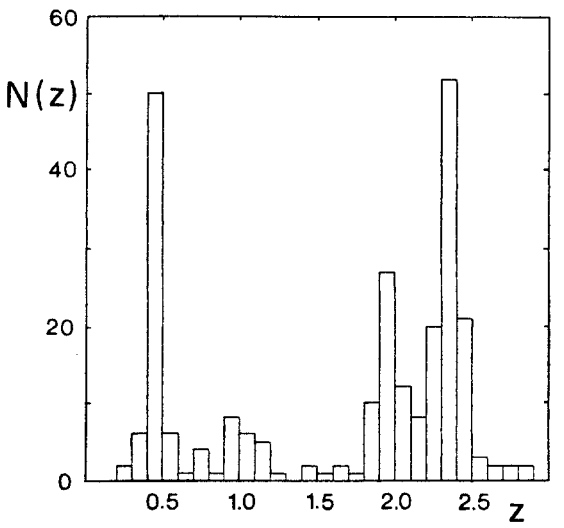

Fig. 7. Histogram of z-values of 255 quasars found in this survey.

5 A census of quasars in field No. 411.

For the quasar candidates in the magnitude range $18^m - 19^m$ redshifts were obtained interactively from the objective prism spectra. The identification of Ly α emission is quite reliable, especially, because in most cases other lines such as N V, Si IV or C IV are also present. The identification of the Mg II emission is more difficult, because no other prominent emission lines appear at the same redshift. When only one strong emission feature was present, the underlying continuum was used as additional criterion; when the strong line appeared on a very blue continuum (attributable to the Lyman continuum), the feature was identified as Ly α, when the continuum appeared flat, the emission-line was assigned to Mg II. Structural criteria, high and narrow for Ly α, low and more diffuse for Mg II, were also used.

255 redshifts were obtained with an average of 2.0 lines per spectrum. Among the objects are 158 with Ly α emission. In these spectra the average is 2.4 lines. These data constitute a well-defined, physically homogeneous sample of quasars in the redshift range $1.9 < z < 2.9$ and absolute magnitudes between -25^m and -27^m (K-corrections are negligible in this range, assuming exponential energy distribution in the spectra).

Figure 5 shows spectra of quasar candidates with Ly α lines found in this survey. In *Fig. 6 a-c* a comparison is made of three spectra of the same quasar. *(a)* shows the uncorrected density objective prism spectrum, *(b)* is the intensity corrected spectrum on a linear wavelength scale, *(c)* shows a slit spectrum taken with EFOSC at the ESO 3.6 m-telescope.

6 Quasar statistics

The z-distribution of all quasars is presented in *Fig. 7*. Most quasars are found at z values near 0.4, where the Mg II emission line appears in the central part of the

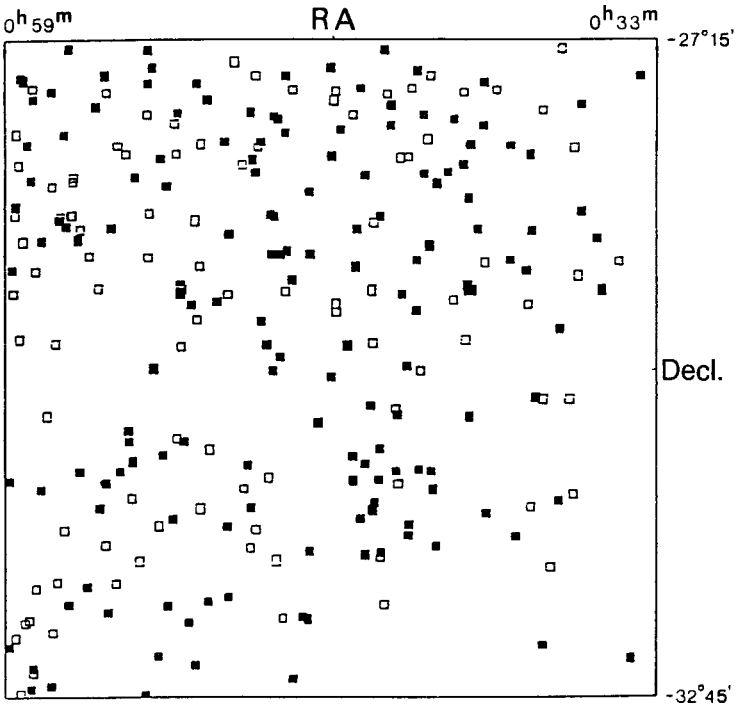

Fig. 8. Distribution of the 255 quasars in ESO/SRC field No. 411. Quasars with Ly α lines are shown as filled squares, all other quasars as open squares.

spectral window, and around $z = 2.4$ with Ly α. For other redshifts, only weak emission lines can be expected, so that it is difficult to find quasars at these values. The peak around $z = 0.4$ may be too high, because Mg II quasars are more uncertain. Because the rest wavelength of Mg II is much larger than the rest wavelength of Ly α, the range of observable z-values for Mg II quasars is much smaller. This explains the narrowness of the peak at small redshifts in the z-histogram as compared to peak at large z-values.

In *Fig. 8* the two-dimensial distribution of all quasars with measured redshifts in field No. 411 is shown. There seems to be an indication of clustering for the Ly α quasars, *e.g.* a concentration in the south-west quadrant.

z-histograms of the Ly α quasars only, arranged in $55' \times 55'$ cells, show an indication of clustering in the same region and at a depth of $z = 2.4$ (*Fig. 9*). Other, minor concentrations are suggested. The relevant positions in the histograms are shaded. The extent of the major "cluster" is of the order $100\,h^{-1}$ Mpc.

The two-dimensional distribution of the quasars was also studied using the angular correlation function $w(\theta)$ given by Hewett (1982). *Fig. 10* shows $w(\theta)$ for the Ly α quasars. The resolution used is 6'. There may be clustering at angles smaller than 1°3 and on a characteristic scale of $100\,h^{-1}$ Mpc. Because of the small number of objects large noise is expected. In order to test whether this could lead to spurious effects,

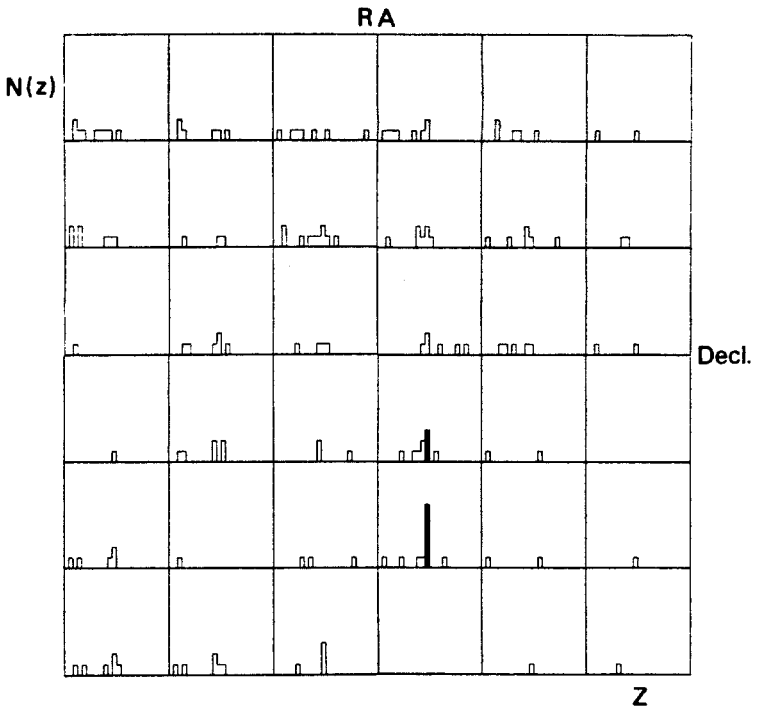

Fig. 9. Histograms of z-values of Ly α quasars in field No. 411, segmented into 36 sections. Ranges: $0 \leq N \leq 10$, $1.8 \leq z \leq 3$, bin size $\Delta z = 0.05$.

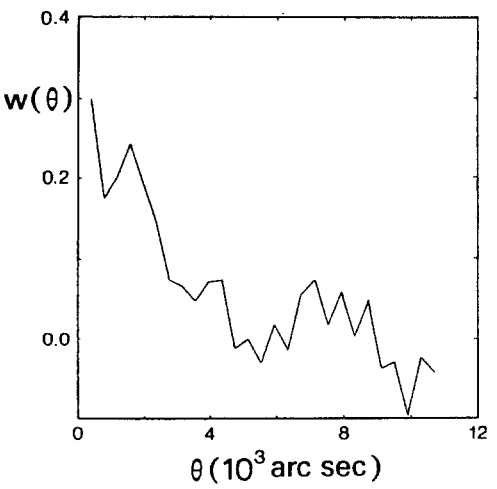

Fig. 10. Two-point correlation function for Ly α quasars.

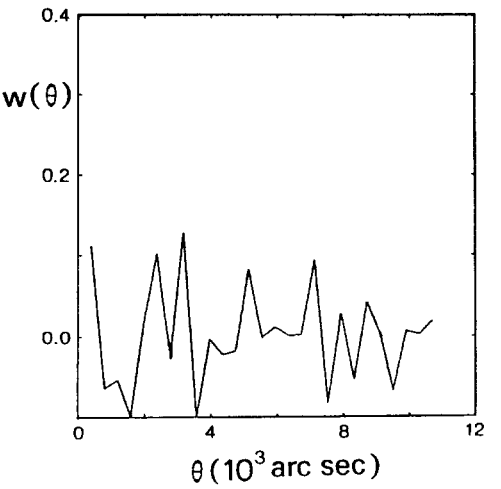

Fig. 11. Two-point correlation function for a random distribution.

the correlation function for random distribution, using the same average number of objects per cell, was determined. The result is shown in *Fig. 11.* Mg II quasars show marginal clustering. This may be attributed to the small number of objects (70), the larger number of misidentifications and/or the absence of clustering. The number of quasars which are neither Ly α nor Mg II quasars is too small for a test.

Data of three more fields have recently become available from the MRSP. With the expected number of about 600 Ly α quasars, we will be able to derive clustering properties from a more reliable homogeneous sample of quasars.

References

Beuermann, K., Clowes, R.G., 1988. *These proceedings*, p. 246.

Clowes, R.G., Smith, M.G., Wallace, P.T., Cannon, R.D., Savage, A., Boksenberg, A., 1980. *Mon. Not. R. astr. Soc.*, **193**, 415.

Clowes, R.G., Cooke, J.A., Beard, S.M., 1984. *Mon. Not. R. astr. Soc.*, **207**, 99.

Foltz, C.B., Chaffee, F.H., Hewett, P., MacAlpine, G.M., Turnshek, D.A., Weymann, R.J., Anderson, S.F., 1987. *Astr. J.*, **94**, 1423.

Hagen, H.E., Engels, D., Groote, D., Reimers, D., 1988. *These proceedings*, p. 233.

Hewett, P.C., 1982. *Mon. Not. R. astr. Soc.*, **201**, 867.

Hewett, P.C., Irwin, M.J., Bunclark, P., Bridgeland, M.T., Kibblewhite, E.J., He, X.T., Smith, M.G., 1985. *Mon. Not. R. astr. Soc.*, **213**, 971.

Hewitt, A., Burbidge, G., 1987. *Astrophys. J. Suppl.*, **63**, 1.

Horstmann, H., 1988, *These proceedings*, p. 111.

Schuecker, P., 1988. *These proceedings*, p. 142.

Véron-Cetty, M.-P., Véron, P., 1987. *A Catalogue of Quasars and Active Nuclei*, 3rd edition, ESO scientific report No. 5.